

Exploring the Adversarial Vulnerabilities of Vision-Language-Action Models in Robotics

Taowen Wang¹, Dongfang Liu¹, James Chenhao Liang^{1,2},
Wenhao Yang³, Qifan Wang⁴, Cheng Han⁵,
Jiebo Luo⁶, Ruixiang Tang⁷

¹Rochester Institute of Technology, ²U.S. Naval Research Laboratory,
³Lamar University, ⁴Meta AI, ⁵University of Missouri - Kansas City,
⁶University of Rochester, ⁷Rutgers University

Abstract

Recently in robotics, Vision-Language-Action (VLA) models have emerged as a transformative approach, enabling robots to execute complex tasks by integrating visual and linguistic inputs within an end-to-end learning framework. While VLA models offer significant capabilities, they also introduce new attack surfaces, making them vulnerable to adversarial attacks. With these vulnerabilities largely unexplored, this paper systematically quantifies the robustness of VLA-based robotic systems. Recognizing the unique demands of robotic execution, our attack objectives target the inherent spatial and functional characteristics of robotic systems. In particular, we introduce an untargeted position-aware attack objective that leverages spatial foundations to destabilize robotic actions, and a targeted attack objective that manipulates the robotic trajectory. Additionally, we design an adversarial patch generation approach that places a small, colorful patch within the camera’s view, effectively executing the attack in both digital and physical environments. Our evaluation reveals a marked degradation in task success rates, with up to a 100% reduction across a suite of simulated robotic tasks, highlighting critical security gaps in current VLA architectures. By unveiling these vulnerabilities and proposing actionable evaluation metrics, this work advances both the understanding and enhancement of safety for VLA-based robotic systems, underscoring the necessity for developing robust defense strategies prior to physical-world deployments.

1. Introduction

“First directive: A robot cannot harm a human or, through inaction, allow a human to be harmed.”

— Finch [78]

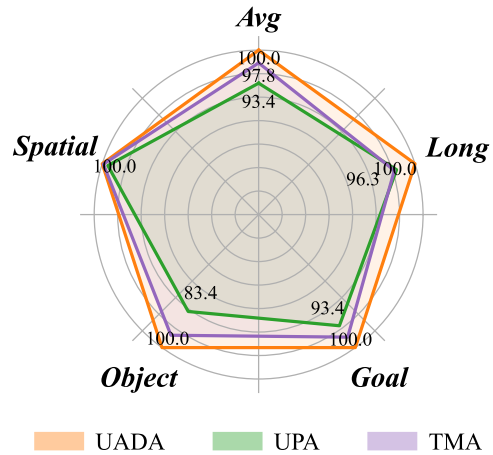


Figure 1. **Fatal failure rates** resulting from different attacking schemes (*i.e.*, UADA, UPA, and TMA) underscore vulnerabilities in VLA-based robotic systems.

In the movie *Finch*, set in a post-apocalyptic future, an intelligent robot navigates complex themes, underscoring the importance of interactive safety with its human master. Once speculative, this portrayal is now increasingly plausible with the rise of visually-conditioned language models (VLMs) [73, 82] capable of seamlessly interpreting both visual and linguistic contexts. A notable realization of this potential can be seen in Vision-Language Action (VLA) models [16, 35, 76, 77], which integrate VLMs into robotic systems to enable end-to-end learning that encompasses both high-level planning and the generation of low-level robot control actions. While VLA models demonstrate a promising step toward generalist robotic intelligence, they also introduce potential vulnerabilities that remain underexplored. This work addresses the pressing need to investigate the new attack surfaces associated with VLA-based robotic systems.

To gain deeper insights into these vulnerabilities, we an-

alyze VLA-based models and general robotic operations, highlighting two key characteristics crucial for designing effective adversarial attacks. First, creating attack objectives for robotic systems requires consideration of the physical dynamics and constraints intrinsic to robotic movement. Conventional adversarial attacks, in this case, often fail to produce significant deviations in intended actions because they disregard these constraints. Second, VLA models generate control signals that function as a time series of *K-class* predictions (see §3.1), making it essential to design attacks that exploit the temporal dependencies within these sequences to cause substantial disruptions in robotic behavior. Achieving attacks that are effective in both digital simulations and real-world environments remains critical yet challenging.

To address these challenges, our work intensifies the adversarial threats posed to VLA-based systems by developing specialized attack objectives and designing effective attack methods. Specifically, we formulate an **Action Discrepancy Objective** aimed at maximizing the normalized action discrepancy within VLA-based robotic systems. This strategy ensures that, at each decision point, the robot’s behavior can diverge from the optimal trajectory. Additionally, we introduce **Geometry-Aware Objective** that considers the robot’s movement in three-dimensional space, characterized by three degrees of freedom. By optimizing the cosine similarity between adversarial and ground-truth directions, we induce deviations in the robot’s movement direction from its intended path, increasing the likelihood of task failure. To achieve these attack objectives, we develop a straightforward yet effective **Patch-Based Attack** targeting VLA-based robotic systems. This approach enables adversarial attacks in both digital and physical settings, revealing substantial vulnerabilities within the VLA-based system.

Together, these innovations yield several significant contributions: ❶ This work presents a pioneering and comprehensive analysis of vulnerabilities within VLA-based robotic systems, a new paradigm for training generalized robotic policies using generative foundation models. We reveal critical threats to adversarial attacks (see Fig. 1), emphasizing the urgent need to enhance robustness before real-world deployment. ❷ We are the first to define attack objectives specific to the powerful VLA model and to employ a straightforward adversarial patch against it (see §3). This offers valuable insights for the research community to explore systemic failures in similar concurrent generative foundation models. ❸ We rigorously evaluate our approach in both simulated and physical environments across four distinct robotic tasks, observing a significant raises in task failure rates of 100% and 43%, respectively. This highlights the effectiveness of our attack strategies (see §4.2).

2. Related work

2.1. AI-driven Generalist Robot

Developing generalist robots [6, 14, 27, 38, 63] requires models not only handle varied interactions but also maintain robustness in unstructured environments. Early intelligent robots [53, 54, 56, 57, 86] relied on rule-based approaches, effective only in controlled settings and requiring extensive reprogramming for new tasks. The advent of deep learning [19, 31, 33, 42, 59] and reinforcement learning [1, 66, 75] has shifted this paradigm to adapt through data, increasing robot versatility and reducing manual reconfiguration.

Recent studies [7, 55, 60] have further advanced the development and potential of large-scale visually-conditioned language models (VLMs) as key enablers for generalist robots, demonstrating promising generalization across a variety of scenes [15, 25, 32, 43, 67, 87]. One of the notable examples is OpenVLA [35], which integrates dual visual encoders with a pre-trained large language model to enable observation-to-action capabilities through instruction-following [10, 34, 47, 48, 73, 85]. By aligning visual and textual semantics, OpenVLA facilitates complex scenario understanding and end-to-end action generation, showing impressive generalization when executing previously unseen task instructions. Despite its success in generalist robotic applications, the vulnerability of such systems remains largely unexplored. This study aims to address this gap by investigating adversarial threats to VLA-based robotic systems.

2.2. Human-Robot Interaction Safety

Current human-robot interaction risks include physical discomfort or injury [4, 5, 22]. Considering these risks, ensuring safety during interactions becomes the top priority as many literature outlined [24, 41, 70]. Existing robotic safety strategies have primarily concentrated on mitigating naturally occurring hazards [41]. These strategies can be generally categorized into pre-collision or post-collision interventions based on the timing of manage hazards [40]. Pre-collision approaches aim to prevent severe hazards by implementing physical constraints, such as controlling force and speed [28, 30], defining safety zones [71] and predicting human actions to avoid potentially dangerous robot movements [36, 37, 52]. Post-collision strategies, on the other hand, focus on detection and response after a harmful action has occurred [20, 50]. While there is substantial research on robotic safety, the integration of AI into robotic policies poses new challenges, where attackers can manipulate AI-driven robot and execute malicious actions. Such threats introduce additional layers of risk and complexity. In this paper, we primarily focus on adversarial threats.

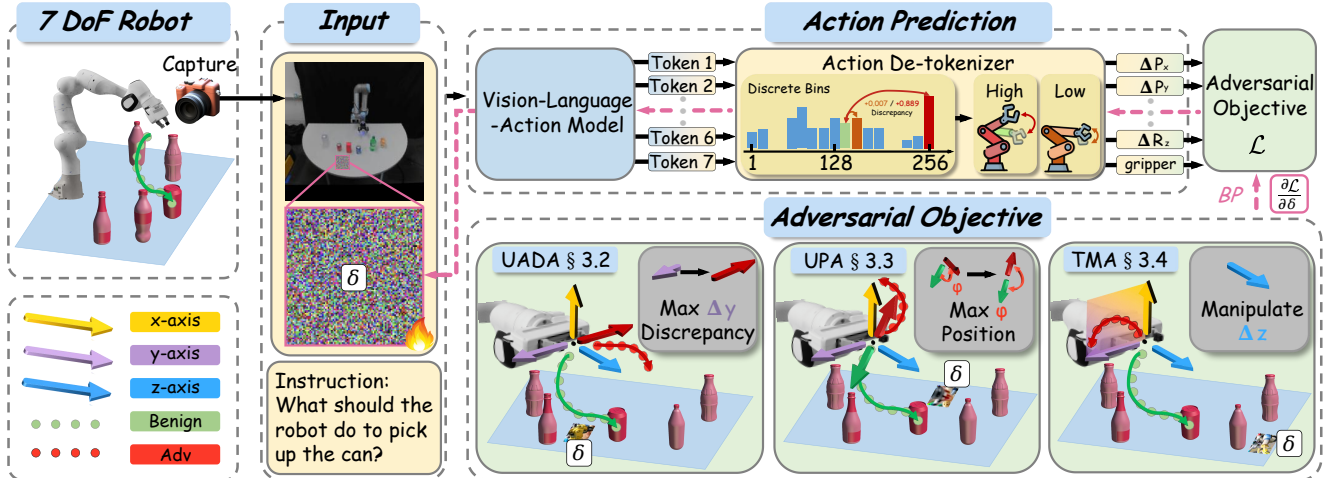


Figure 2. **Overall Adversarial Framework.** The robot captures an input image, processes it through a vision-language model to generate tokens representing actions, and then uses an action de-tokenizer for discrete bin prediction. The model is optimized with adversarial objectives focusing on various discrepancies and geometries (*i.e.*, UADA, UPA, TMA). Forward propagation is shown in black, and backpropagation is highlighted in pink. These objectives aim to maximize errors and minimize task performance, with visual emphasis on 3D-space manipulation and a focus on generating adversarial perturbation δ during task execution, such as picking up a can.

2.3. Adversarial Attacks in Robotics

Adversarial attacks serve as critical tools for assessing model vulnerabilities, particularly in robotics, where models operate in dynamic, real-world settings. Traditional gradient-based, pixel-level attacks [17, 21, 45, 51, 64, 74] exploit model gradients to calculate malicious perturbations, achieving high attack success rates in digital environments. For physical-world attacks, patch-based methods [3, 8, 62, 79, 80] offer a practical alternative for real-world applications by introducing physically realizable perturbations that retain efficacy under varied conditions, such as angle or lighting changes, making them highly applicable for robotic systems. Therefore, considering VLA-based models enable robot execution in real-world scenarios, this work employs a patch-based attack strategy.

VLA models [13, 26, 67] couple visual and linguistic modalities for perception-action alignment. The continuous, high-dimensional nature of visual inputs [51, 61, 65] makes them the most likely target for adversarial perturbations, as attackers can subtly alter visual data in ways that are difficult to detect [2, 9, 68]. Consequently, this work applies attacks on the visual modality to achieve robust manipulations across diverse environments. To the best of our knowledge, this study is one of the earliest attempts to formally define adversarial objectives for VLA models, targeting gaps in adversarial robustness through the model’s geometric constraints (*e.g.*, spatial dependencies in visual input) and architectural nuances (*e.g.*, cross-modal information integration).

3. Methodology

This section outlines our proposed methodology. We first review the core algorithmic principles of VLA in §3.1, which

serves as the foundation for the adversarial scheme designs. We then present two types of untargeted adversarial attacks, including Untargeted Action Discrepancy Attack (UADA) in §3.2 and Untargeted Position-aware Attack (UPA) in §3.3. In §3.4, we further include Targeted Manipulation Attack (TMA), designed to direct the robot toward specific erroneous execution. The implementation details are presented in §3.5. The overall framework is shown in Fig. 2.

3.1. Preliminary

Vision-Language Action models [35, 87] (see Fig. 2) are built on large language models integrated with visual encoders, enabling robots to interpret human instructions and process visual input from a camera to perform context-aware actions. VLA models [35, 44, 87] generally abstract continuous action prediction into a classification problem by discretizing robot actions. Specifically, they first discretize the continuous probabilities into class labels $c = \arg \max F(x)$. An action de-tokenizer then generates actions $y = DT(c)$. By categorizing action values into discrete class labels, the model converts continuous probability outputs into discrete signals, this simplification facilitates quicker convergence and faster training times, and is commonly used for VLA-based models [35, 44, 87].

In this work, we focus on a 7-degree-of-freedom (DoF) robotic arm [23]. At each step, an action consists of 7DoFs with specific physical significance in three-dimensional Cartesian space, represented by:

$$A = [\Delta P_x, \Delta P_y, \Delta P_z, \Delta R_x, \Delta R_y, \Delta R_z, \text{gripper}], \quad (1)$$

where $\Delta P_{x,y,z}$ and $\Delta R_{x,y,z}$ denote relative positional and rotational changes along the x-, y-, and z-axis, discretized

into 256 uniform bins across the action range [35]. The *gripper* state is binary, indicating its open or closed state. This control design presents a unique challenge for adversarial attacks, as finely divided bins result in minimal action discrepancies between neighboring bins (e.g., $\pm 0.007/\text{bin}$). This means that even if an attack shifts the classification to an adjacent bin, the resulting action discrepancy has minimal impact real-world performance.

3.2. Untargeted Action Discrepancy Attack

We first focus on maximizing action discrepancies by introducing Untargeted Action Discrepancy Attack (UADA). This attack is based on the observation that larger robot actions usually correlate with intense physical movements, which, in turn, may amplify the potential for real-world hazards [28–30]. Specifically to UADA, the attack target is one or combination of 7DoFs, defined as $y^I = \{y^i | i \in [1, \dots, 7]\}$. To define UADA’s objective, we first determine the maximum action discrepancy d_{\max} , which represents the largest deviation that can occur within the allowed range for each DoF. This is calculated by measuring the distance between the ground truth y and its action range $[y_{\min}, y_{\max}]$ as:

$$d_{\max}^i(y) = \max(|y^i - y_{\min}^i|, |y^i - y_{\max}^i|). \quad (2)$$

We next calculate the applied action discrepancy $d_{\text{applied}}^i(x, y) = |F(x)^i - y^i|$ in order to measure the deviation between the model’s output and the ground truth, where $F(x)^i$ is the i -th action output of model $F(x)$. In this sense, we can evaluate the Normalized Action Discrepancy (NAD) as the drifting ratio between d_{applied}^i and d_{\max}^i as:

$$\text{NAD} = \frac{1}{I} \sum_i d_{\text{applied}}^i / d_{\max}^i. \quad (3)$$

Since VLA models are currently operated via predicting discrete token labels (see §3.1), we then need to bridge action discrepancy derived from these discrete labels into learnable targets. Specifically, we weighted sum the model output probabilities across J bins by their own class label j as:

$$d_{\text{applied}}^{\prime i}(x, y) = \left| \sum_{j=1}^J (j \cdot \mathcal{F}(x)_j^i) - c^i \right|, \quad (4)$$

where $\mathcal{F}(\cdot)_j^i$ is the model output probability of i -th DoF’s j -th bin. Finally, the attack objective for UADA is defined as minimizing the ratio of weighted sum $d_{\text{applied}}^{\prime i}$ to $d_{\max}^i(y^i)$:

$$\mathcal{L}_{\text{UADA}} = \mathbb{E}_{(x, y) \sim \mathcal{X}} \left[\sum_i \frac{d_{\text{applied}}^{\prime i}(x + \delta, y)}{d_{\max}^i(y)} \right]^{-1}, \quad (5)$$

where x, y is a benign image and action pair, sampled from distribution \mathcal{X} . UADA defines the objective functions tailored for the robot’s action space, allowing adversarial

patches to create significant, lasting disruptions in task performance. In this design, we uniquely leverage the model’s discrete action structure to design attacks that amplify meaningful discrepancies in robot behavior.

3.3. Untargeted Position-aware Attack

We further extend untargeted adversarial attacks to consider the positional dynamics within VLA models. In typical task execution, precise and directed movements of the end-effector towards designated goals are essential, with actions mapped in three-dimensional space. The positional degrees of freedom, $y^{\text{pos}} = [y^1, y^2, y^3]$ encapsulates the directional movements within 3D for effective robotic control.

Recognizing the importance of y^{pos} in controlling the end-effector’s path, we introduce a position-aware attack to disrupt the intended movement trajectory. This type of adversarial vulnerability remains largely unexplored but has significant implications for task failure: the attack objective can steer the end-effector away from its intended path by introducing directional perturbations, amplifying errors and causing substantial trajectory distortions. Formally, we define the Untargeted Position-aware Attack (UPA) objective as:

$$\mathcal{L}_{\text{UPA}} = \mathbb{E}_{(x, y) \sim \mathcal{X}} \left[\alpha \frac{y_{\text{adv}}^{\text{pos}} \cdot y^{\text{pos}}}{\|y_{\text{adv}}^{\text{pos}}\| \|y^{\text{pos}}\|} + \beta \frac{1}{\|y_{\text{adv}}^{\text{pos}} - y^{\text{pos}}\|_2} \right], \quad (6)$$

where α and β are the hyperparameters that balance between the directionality and magnitude of the perturbations. By integrating geometric awareness into our attack, this approach generates perturbations that induce cumulative deviations in the robot’s trajectory, even with minimal adjustments. L_2 -normalization $\|\cdot\|_2$ further intensifies these deviations, rendering the attack highly effective and disruptive.

Algorithm 1: Adversarial Patch Attack.

- 1: **Input:** \mathcal{X} : dataset; δ : adversarial patch; \mathcal{L}_o : objective function; \mathcal{F} : vision language action model; $\mathcal{T}(\cdot)$: Transformation; ϕ, ψ are two hyperparameters for transformation; T : maximum iteration steps; k : maximum inner-loop steps.
 - 2: **Initialize:** $\delta \sim \mathcal{U}[0, 1]$, $\mathcal{L}_o \in \{\mathcal{L}_{\text{UADA}}, \mathcal{L}_{\text{UPA}}, \mathcal{L}_{\text{TMA}}\}$
 - 3: **for** $i = 1, 2, \dots, T$ **do**
 - 4: $(x, y) \sim \mathcal{X}$
 - 5: **for** $i = 1, 2, \dots, k$ **do**
 - 6: $shx, shy \sim \mathcal{U}(-\phi, \phi)$, $\theta \sim \mathcal{U}(-\psi, \psi)$
 - 7: $y_{\text{pred}} \leftarrow \mathcal{F}(\mathcal{T}(x + \delta))$ {▷ Feedforward }
 - 8: $\frac{\partial \mathcal{L}_o}{\partial \delta} \leftarrow \mathcal{L}_o(y_{\text{pred}}, \cdot)$ {▷ Backpropagation }
 - 9: $\delta \leftarrow \frac{\partial \mathcal{L}_o}{\partial \delta}$ {▷ Update }
 - 10: Clip δ into normal pixel range.
 - 11: **end for**
 - 12: **end for**
-

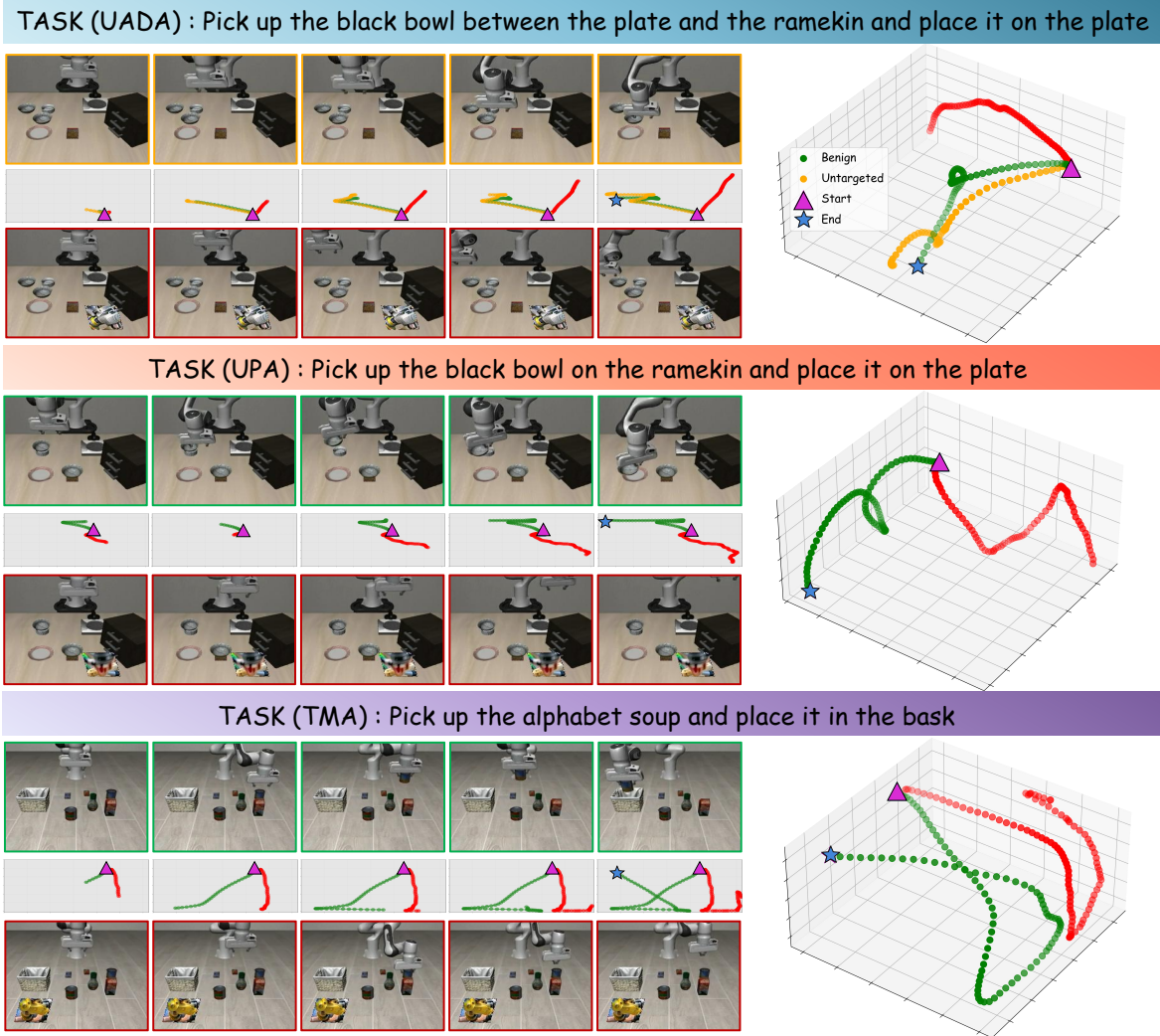


Figure 3. **Qualitative Results** of adversarial vulnerabilities over OpenVLA-7B [35] and OpenVLA-7B-LIBERO [35] with objectives of UADA, UPA, and TMA, respectively. We visualize the overall 3D trajectories and 2D trajectories of benign ● and adversarial ● scenarios at each time step to compare the impact of the generated adversarial patch in affecting them. The untargeted trajectory ● is visualized in UADA task. All trajectories start with ▲, and we plot the success end point, marked as ★.

3.4. Targeted Manipulation Attack

In addition to the aforementioned untargeted attacks, we also explore the adversarial vulnerabilities of VLA models with a targeted strategy. This attack aims to mislead the models into predicting specific trajectories, resulting in precise alterations. These targeted alterations can potentially drive malicious behaviors or induce task failure. The objective of the targeted manipulation attack is:

$$\mathcal{L}_{TMA} = \mathbb{E}_{(x,y) \sim \mathcal{X}} [\mathcal{H}(\mathcal{F}(x + \delta), y_T^I)], \quad (7)$$

where $y_T^I = \{y^i = t | i \in [1, \dots, 7], t \in \mathcal{R}\}$ represents the adversarial target; and $\mathcal{H}(\cdot, \cdot)$ denotes the Cross-Entropy loss, which measures the error between the predicted state under adversarial perturbation and the desired target state. By steering the robot towards an adversarial target across

successive time steps, our approach manipulates the trajectory and undermines task performance, ultimately leading to a substantial disruption of intended operations. Furthermore, manipulating any individual DoF or a combination thereof can also severely compromise task success, given that the errors in one dimension tend to propagate and magnify over time during execution (see Fig. 3).

3.5. Implementation Details

The implementation of our pipeline is detailed in Algorithm 1. We incorporate two key modifications to enhance the training stability of the generated patch.

Inner-loops. Following previous work [51], we add k inner-loops optimize steps during each iteration in line 5, aiming to reduce data variance and ensure more consistent updates.

Geometric Transformations. To improve the robustness of our attack under real-world scenarios, we employ random geometric transformations $\mathcal{T}(\cdot)$ in line 7 with affine and rotation transformations [3] as:

$$\mathcal{T}(\cdot) = \begin{bmatrix} 1 & sh_y \\ sh_x & 1 \end{bmatrix} \cdot \begin{bmatrix} \cos \theta & -\sin \theta \\ \sin \theta & \cos \theta \end{bmatrix}, \quad (8)$$

where $sh_x, sh_y \sim \mathcal{U}(-\phi, \phi)$ are shear factors, and $\theta \sim \mathcal{U}(-\psi, \psi)$ denotes the rotation angle, both sampled from uniform distributions during inner loop optimization step k .

4. Experiments

In this section, we present the experimental design outlined in §4.1 and report the quantitative and qualitative results of UADA, UPA, and TMA in both simulation and physical-world scenarios (§4.2). We then analyze diagnostic experiments (§4.3) to evaluate the influence of key components. Additionally, we assess the robustness of our method against various defense mechanisms in §4.4 and conclude with a comprehensive systemic discussion in §4.5.

4.1. Experiment Setup

Simulation Tasks. We conduct simulation attacks on BridgeData V2 [72] and LIBERO [46]. BridgeData V2 [72] is a real-world dataset comprising 24 diverse environments and 13 distinct skills, such as grasping, placing, and object rearrangement, with a total of 60,096 trajectories. LIBERO [46] is a simulation dataset designed to evaluate models across four distinct task types (Spatial, Object, Goal, Long), each containing 10 tasks with 50 human-teleoperated demonstrations. Notably, LIBERO-Long combines diverse objects, layouts, and long-horizon tasks, making them challenging for complex, multi-step planning, thus we choose LIBERO-Long to conduct UADA, UPA and TMA.

Robot Setups. For the physical-world tasks, we adopt a robotic system consisting of a **Universal Robots UR10e** equipped with a **Robotiq Hand-E Gripper** to provide a 7DoF motion. The sensing system includes one RGB webcam in the fixed position with a shoulder view.

Victim VLA Models. In our study, we select publicly available and current most influential VLAs as victim models for evaluation. Specifically, we focus on four variants of the OpenVLA model, each trained independently on different tasks within the LIBERO dataset (*i.e.*, Spatial, Object, Goal, Long). To evaluate the effectiveness of our methods, we craft adversarial patches using two distinct generating setups. The first involves a model trained in a **simulated** environment using the LIBERO dataset [46] with the openvla-7B-libero-long variant [35]. The second uses a model trained on **physical** world data from the BridgeData v2 dataset [72] with the openvla-7B model [35]. This approach allows us to assess our methods on both simulated and real-world data. Subsequently, we evaluate the performance of generated adversarial patches on victim models (*i.e.*, OpenVLA LIBERO

Table 1. **Untargeted results (Simulation).** We report Failure rates (%) and NAD (%) in LIBERO simulation. * denotes the in-domain victim model and dataset aligned with the patch generation model and dataset, Δ denotes a transfer attack task involving a distinct victim model and dataset (see §4.1). The naive FR of each victim model in the corresponding task is: Spatial (15.3%), Object (11.6%), Goal (20.8%) and Long (46.3%). The FR (\uparrow) is highlighted in **best** and second best. Same for Tab. 2.

Objective	Attack Actions	NAD (%)	Victim models			
			Spatial Δ	Object Δ	Goal Δ	Long*
Untarget	DoF ₁	14.1	100.0	100.0	100.0	100.0
	DoF ₁₋₃	11.4	100.0	100.0	100.0	100.0
UADA	DoF ₁	18.1	100.0	100.0	100.0	100.0
	DoF ₁₋₃	14.3	100.0	100.0	100.0	100.0
UPA	DoF ₁₋₃	<u>14.5</u>	100.0	83.4	93.4	96.7

variants) trained on different tasks to rigorously prove the robustness and effectiveness of our method. These models are trained with distinct data sources and task objectives. Additional results on transferability (*e.g.*, LLaRA [44]) are included in §S1.

Attacking Details. Aligned with the former objective [69] aiming to mislead classifiers and combine with our framework, we design and conduct an untargeted attack. Following [35], we apply scaling and normalization for data pre-processing. The initial learning rate is set to $2e^{-3}$, with the AdamW optimizer [49] with a cosine annealing scheduler, including 20 warm-up iterations. Training is conducted over $2e^3$ iterations with a batch size of 6 and 50 inner-loop steps (see Algorithm 1). The transformation parameters a, b in Eq. 8 are set to 0.2 and 30 to simulate real-world perspective change. For all three objectives, considering the trade-off between stealth and performance observed in §S2, we set the patch size to 5%. For the hyperparameters α, β in Eq. 6, We conduct grid search and tune α from [0.2, 0.4, 0.6, 0.8] and β from [0.8, 0.6, 0.4, 0.2]. We select $\alpha = 0.8$ and $\beta = 0.2$ based on the validation set performance. Ablation studies *w.r.t.* α and β are presented in §S6.

Table 2. **Untargeted results (Physical).** Transfer results to 4 victim models with adversarial patches generated from physical data and corresponding model.

Objective	Attack Actions	NAD (%)	Victim model			
			Spatial Δ	Object Δ	Goal Δ	Long Δ
Untarget	DoF ₁	26.7	85.4	56.4	77.3	65.8
	DoF ₁₋₃	23.8	78.1	46.7	52.4	56.7
UADA	DoF ₁	31.9	73.4	33.5	41.7	62.3
	DoF ₁₋₃	26.4	<u>85.9</u>	<u>49.5</u>	32.1	<u>60.5</u>
UPA	DoF ₁₋₃	<u>26.9</u>	86.4	42.7	<u>53.3</u>	61.2

Evaluation Details. To assess the effectiveness and robustness of our methods, we conduct evaluations on the LIBERO dataset [46]. Each task suite is evaluated with 10 trials, with fixed patch location (see §S5) This setup is for avoiding the patch obstructing task-related objects.

Building on the concept of robotic tasks Success Rate

Table 3. **Targeted Manipulation Attack results.** Average failure rate (%) are reported in 4 LIBERO simulation tasks. The performance of AFR (\uparrow) is marked in **best** and second best. The initial AFR across the four tasks is 23.5%.

Generation Setup	Metric	Target Actions			
Simulation	/	DoF ₁	DoF ₂	DoF ₃	DoF ₄ ...
	L1	0.022	0.029	0.040	0.029
	AFR	97.8	<u>97.5</u>	96.8	73.4
	/	... DoF ₅	DoF ₆	DoF ₇	DoF ₁₋₃
	L1	0.024	0.023	0.046	0.031
	AFR	96.8	88.3	84.1	95.5
Physical	/	DoF ₁	DoF ₂	DoF ₃	DoF ₄ ...
	L1	0.013	0.022	0.041	0.031
	AFR	89.1	85.3	57.2	48.8
	/	... DoF ₅	DoF ₆	DoF ₇	DoF ₁₋₃
	L1	0.032	0.018	0.049	0.027
	AFR	54.3	46.2	57.8	<u>86.8</u>

(SR) introduced in LIBERO [46], we adopt Failure Rate (FR), defined as $1 - \text{SR}$, as the primary evaluation metric for this study. To further quantify action discrepancy, we employ NAD (see Eq. 3) for untargeted attacks, as it considers relative distances to quantify deviation from the optimal action. A higher NAD value indicates a greater discrepancy between the ground truth and the predicted action. For targeted attacks, we utilize the L1 distance, which measures the absolute deviation from the specified target action.

Reproducibility. Our methods are implemented in Pytorch [58]. Experiments are conducted on a single NVIDIA A100-40GB GPU. Our code and attack video is available at <https://anonymous.4open.science/r/roboticAttack-56FF>.

4.2. Main Result

Quantitative Results. For UADA and UPA, our methods effectively amplify action discrepancies, leading to a notable transfer attack ability in increasing failure rates (see Tab. 1). Specifically, for the **Simulation** setup, UADA and UPA achieve maximum NAD of 18.1% and 14.5%, significantly outperforming untargeted scenarios with increment of 3.8% and 0.4%, respectively. Both untargeted and UADA successfully disrupt the robot execution, with a failure rate to 100%. UPA also results in a significant increment compared to the failure rate of the victim methods in benign scenarios, which is 100% *v.s.* 15.3%, 83.4% *v.s.* 11.6%, 93.4% *v.s.* 20.8% and 96.7% *v.s.* 46.3%, respectively. Regarding the **Physical** setup, both UADA and UPA generate actions with large action discrepancies, which are 31.9% and 26.9% with an increase of 5.2% and 0.2% compared to the best 26.7% in untargeted scenarios, respectively. UPA demonstrates an improvement of 86.4% *v.s.* 85.9% over the spatial task compared to untargeted.

For TMA task, we evaluate the effectiveness of our method by manipulating various DoF to 0. Our method demonstrates significant effectiveness in manipulating robotic trajectory and increasing failure rates (see Tab. 3). Specifically, when applied to the different generation settings, our approach yields notable increments across various tasks, including an max average failure rate 97.8% *v.s.* 23.5% of benign performance in **Simulation**, and 89.1% in **Physical**, respectively. To further prove the generalizability, we target attack on several non-zero values in §S2.

Qualitative Results. We qualitatively analyze the trajectories of robot movement of the proposed three different objectives in Fig. 3. For UADA, we compare the trajectory deviations in the same trail with patch generated from UADA and untarget attack. As seen, the untarget attack induces small deviations in the trajectory UADA, on the other hand, produces significantly larger trajectory deviations (also supported by NAD metric in Tab. 2), which is attributed to UADA’s capability of incorporating action discrepancies. In our observation, UADA significantly amplifies the effect on overall task execution, thereby increasing the potential for robotic hazards. For UPA, we observe chaotic and irregular behaviors, including instances where the end-effector moves out of the camera’s field of view. We attribute this phenomenon to the efficacy of the adversarial patch in perturbing the model’s spatial perception, inducing a consistent deviation from the intended direction of movement, ultimately resulting in failure in a long run.

For TMA, we observe a notable reduction in the range of motion along the x-axis corresponding to the targeted attack axis. This suggests that our proposed targeted attack can effectively constrained robot movements.

In summary, the qualitative analysis shows that both Untarget attack, UADA, UPA, and TMA can effectively disrupt the robot actions generated from VLA models. These findings underscore a *pressing security concern* during the deployment of generalist robots, especially when considering application scenes that requires reliable operations [11, 71].

Physical-world Performance. In addition to the digital simulation results, we also conduct a comprehensive evaluation of the performance of our generated adversarial patches in physical-world testing scenarios. The evaluation encompassed 100 trials across three distinct tasks: object grasping, placement, and manipulation (see §S3 for more details). As shown in Fig. 5, the adversarial patch generated with UADA demonstrated the ability to manipulate the robot effectively, achieving an attack success rate exceeding **43%**. Although this success rate is lower than the corresponding digital-world performance (*i.e.*, **85.9%**), it highlights the effectiveness of our patches in physical-world applications as well without the need for further adaptations. Crucially, we observed that the induced erratic movements (similar to simulation scenario) of the robotic manipulators during

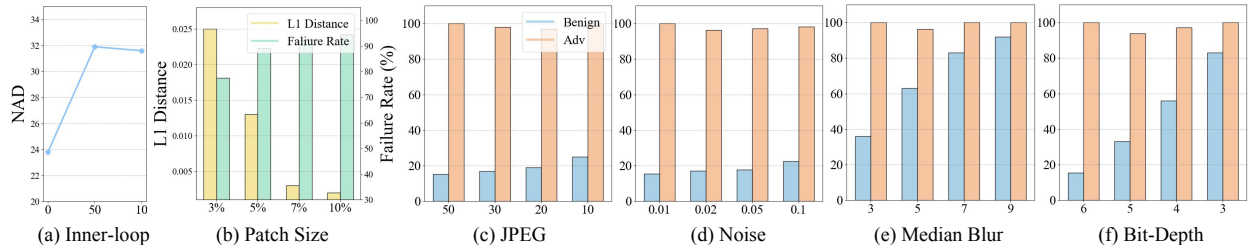


Figure 4. **Impact of Inner-loop, Patch Size and Defense Discussion.** The figure shows how varying Inner-loop affects NAD in UADA, and patch sizes affect L_1 distance and the failure rates in TMA, both targeting at DoF₁. (a) Impact of Inner-loop, (b) Impact of Patch Size and (c-f) the effect of four different defenses on failure rates.

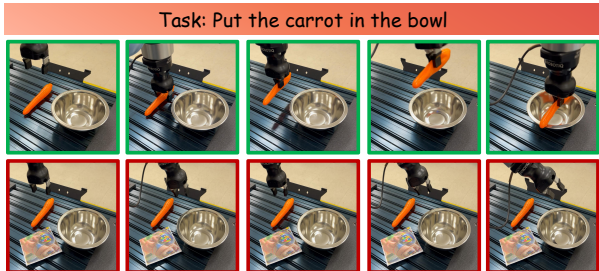


Figure 5. **Qualitative Results** of the physical world. The first/second row show **benign** and **adversarial** cases respectively.

successful attacks pose significant risks to human safety and surrounding environments. This finding emphasizes the severe threat posed by VLA models in real-world applications, consistent with similar observations in digital settings.

4.3. Diagnostic Experiment

We ablate components of our method in this section.

Impact of Inner-loops. We discuss the impact of inner-loop steps to model performance in Fig. 4(a). The results show that NAD first improves when inner-loop steps continue to increase. This is due to the reduced data variance and gradually stabilized gradients. However, further increasing the steps results in a slower performance increase, with a noticeably longer training schedule. We thus choose inner-loop steps=50 as it balances between performance and scale.

Impact of Patch Size. We further study TMA’s performance with different patch sizes, and report the average failure rate across four LIBERO [46] benchmark tasks in Fig. 4(b). The patch sizes examined were [3%, 5%, 7%, 10%] of a 224×224 input image. Our findings indicate an inversely proportional relationship between the L_1 distance of predicted actions and the target action as the patch size increased. This increase in patch size also correlated with a marked rise in task failure rates. The observed trend suggests that larger patch sizes afford the adversary more extensive optimization space to influence the model’s output, which is consistent with previous work [12, 84].

4.4. Robustness Evaluation

We further examine if concurrent defense strategies [18, 81, 83] can generalize against our adversarial examples introduced within VLA. Specifically, we applied four prior defense techniques, and reported their task failure rates for



Figure 6. **Patch Visualization.** Sematic-rich patches generated from physical or simulation datasets.

both benign and adversarial samples in Fig. 4, respectively. The results indicate that our adversarial attack can escape from most of the defense strategies. More details of defense parameters see in §S7.

4.5. Systemic Discussion

Patch Pattern Analysis. In Fig.6, we present the adversarial patches generated for a range of targets. A particularly noteworthy observation is that some of these patches bear a striking resemblance to the structural joints of a robotic arm. Given the strong similarity between these patches and robotic arms in appearance, we hypothesize that these VLA-based models, in their current training paradigms, are often limited to a single robotic system operating within restricted camera views. This constrained perspective/camera pose may inadvertently induce a learned representation bias, where adversarial perturbations align with prominent structural features of the training robot’s appearance in order to deceive current victim models. Given that these patches are model-specific and reflect the spatial and visual patterns of the training environment, we have a reasonable concern that they may compromise VLA-based models’ generalizability and robustness in physical-world deployments.

Possible Defense Strategies. Our work highlights the pressing need for a paradigm shift in the VLA-based models’ training strategies in order to successfully defend our attacks. Specifically, future approaches might incorporate more training scenarios that involve complex multi-robot interactions to mitigate the current patch bias. Another possible solution is to leverage the logical relationships within the robot arm’s physical structure to estimate the actual position of each joint. By predicting joint positions deviated from physical constraints, we can eliminate unreasonable adversarial samples, even if they are similar to actual joint(s).

5. Conclusion

While VLA models have gained significant popularity due to their substantial robot capabilities, this study, for the first time, establishes specific robotic attack objectives and demonstrates that these models are in fact vulnerable to various types of attacks. Experimental results demonstrate that our attacks expose significant vulnerabilities to VLA models, raising concerns regarding impetuous real-world deployments. We believe our framework provides pioneering and foundational contributions to the reliability of AI enhanced robotic systems.

6. Acknowledgements

This research was supported by the National Science Foundation under Grant No. 2242243. The views and conclusions contained herein are those of the authors and should not be interpreted as necessarily representing the official policies or endorsements, either expressed or implied, of U.S. Naval Research Laboratory (NRL) or the U.S. Government. The U.S. Government is authorized to reproduce and distribute reprints for Government purposes notwithstanding any copyright notation herein.

References

- [1] Mokhaled NA Al-Hamadani, Mohammed A Fadhel, Laith Alzubaidi, and Balazs Harangi. Reinforcement learning algorithms and applications in healthcare and robotics: A comprehensive and systematic review. *Sensors*, 24(8):2461, 2024. 2
- [2] Anish Athalye, Nicholas Carlini, and David A. Wagner. Obfuscated gradients give a false sense of security: Circumventing defenses to adversarial examples. In *ICML*, 2018. 3
- [3] Anish Athalye, Logan Engstrom, Andrew Ilyas, and Kevin Kwok. Synthesizing robust adversarial examples. In *ICML*, 2018. 3, 6
- [4] Lefteris Benos, Avital Bechar, and Dionysis Bochtis. Safety and ergonomics in human-robot interactive agricultural operations. *Biosystems Engineering*, 200:55–72, 2020. 2
- [5] Nicole Berx, Wilm Decré, Ido Morag, Peter Chemweno, and Liliane Pintelon. Identification and classification of risk factors for human-robot collaboration from a system-wide perspective. *Computers & Industrial Engineering*, 163:107827, 2022. 2
- [6] Aude Billard and Danica Kragic. Trends and challenges in robot manipulation. *Science*, 364(6446), 2019. 2
- [7] Anthony Brohan, Noah Brown, Justice Carbajal, Yevgen Chebotar, Joseph Dabis, Chelsea Finn, Keerthana Gopalakrishnan, Karol Hausman, Alexander Herzog, Jasmine Hsu, Julian Ibarz, Brian Ichter, Alex Irpan, Tomas Jackson, Sally Jesmonth, Nikhil J. Joshi, Ryan Julian, Dmitry Kalashnikov, Yuheng Kuang, Isabel Leal, Kuang-Huei Lee, Sergey Levine, Yao Lu, Utsav Malla, Deeksha Manjunath, Igor Mordatch, Ofir Nachum, Carolina Parada, Jodilyn Peralta, Emily Perez, Karl Pertsch, Jornell Quiambao, Kanishka Rao, Michael S. Ryoo, Grecia Salazar, Pannag R. Sanketi, Kevin Sayed, Jaspier Singh, Sumedh Sontakke, Austin Stone, Clayton Tan, Huang T. Tran, Vincent Vanhoucke, Steve Vega, Quan Vuong, Fei Xia, Ted Xiao, Peng Xu, Sichun Xu, Tianhe Yu, and Brianna Zitkovich. RT-1: robotics transformer for real-world control at scale. In *Robotics: Science and Systems XIX*, 2023. 2
- [8] Tom B. Brown, Dandelion Mané, Aurko Roy, Martín Abadi, and Justin Gilmer. Adversarial patch. *arXiv preprint arXiv:1712.09665*, 2018. 3, 13
- [9] Nicholas Carlini and David A. Wagner. Adversarial examples are not easily detected: Bypassing ten detection methods. In *Proceedings of the 10th ACM Workshop on Artificial Intelligence and Security*, pages 3–14, 2017. 3
- [10] Xi Chen, Xiao Wang, Lucas Beyer, Alexander Kolesnikov, Jialin Wu, Paul Voigtlaender, Basil Mustafa, Sebastian Goodman, Ibrahim Alabdulmohsin, Piotr Padlewski, et al. Pali-3 vision language models: Smaller, faster, stronger. *arXiv preprint arXiv:2310.09199*, 2023. 2
- [11] Shen Cheng and BS Dhillon. Reliability and availability analysis of a robot-safety system. *Journal of Quality in Maintenance Engineering*, 17:203–232, 2011. 7
- [12] Zhiyuan Cheng, Cheng Han, James Liang, Qifan Wang, Xianguyu Zhang, and Dongfang Liu. Self-supervised adversarial training of monocular depth estimation against physical-world attacks. *arXiv preprint arXiv:2406.05857*, 2024. 8
- [13] Hao-Tien Lewis Chiang, Zhuo Xu, Zipeng Fu, Mithun George Jacob, Tingnan Zhang, Tsang-Wei Edward Lee, Wenhao Yu, Connor Schenck, David Rendleman, Dhruv Shah, et al. Mobility vla: Multimodal instruction navigation with long-context vlms and topological graphs. *arXiv preprint arXiv:2407.07775*, 2024. 3
- [14] Jinda Cui and Jeff Trinkle. Toward next-generation learned robot manipulation. *Sci. Robotics*, 6(54):9461, 2021. 2
- [15] Yiming Cui, Cheng Han, and Dongfang Liu. Collaborative multi-task learning for multi-object tracking and segmentation. *Journal on Autonomous Transportation Systems*, 1:1–23, 2024. 2
- [16] Pengxiang Ding, Han Zhao, Wenjie Zhang, Wenxuan Song, Min Zhang, Siteng Huang, Ningxi Yang, and Donglin Wang. Quar-vla: Vision-language-action model for quadruped robots. In *ECCV*, 2025. 1
- [17] Andrew Du, Bo Chen, Tat-Jun Chin, Yee Wei Law, Michele Sasdelli, Ramesh Rajasegaran, and Dillon Campbell. Physical adversarial attacks on an aerial imagery object detector. In *WACV*, 2022. 3
- [18] Gintare Karolina Dziugaite, Zoubin Ghahramani, and Daniel M. Roy. A study of the effect of JPG compression on adversarial images. *arXiv preprint arXiv:1608.00853*, 2016. 8, 15
- [19] Chelsea Finn, Tianhe Yu, Tianhao Zhang, Pieter Abbeel, and Sergey Levine. One-shot visual imitation learning via meta-learning. In *CoRL*, 2017. 2
- [20] Saskia Golz, Christian Osendorfer, and Sami Haddadin. Using tactile sensation for learning contact knowledge: Discriminate collision from physical interaction. In *ICRA*, 2015. 2

- [21] Ian J. Goodfellow, Jonathon Shlens, and Christian Szegedy. Explaining and harnessing adversarial examples. In *ICLR*, 2015. 3
- [22] Jérémie Guiochet, Mathilde Machin, and H el ene Waeselynck. Safety-critical advanced robots: A survey. *Robotics Auton. Syst.*, 94:43–52, 2017. 2
- [23] Sami Haddadin, Sven Parusel, Lars Johannsmeier, Saskia Golz, Simon Gabl, Florian Walch, Mohamadreza Sabaghian, Christoph J ahne, Lukas Hausperger, and Simon Haddadin. The franka emika robot: A reference platform for robotics research and education. *IEEE Robotics & Automation Magazine*, 29:46–64, 2022. 3
- [24] Roni-Jussi Halme, Minna Lanz, Joni K am ar ainen, Roel Pieters, Jyrki Latokartano, and Antti Hietanen. Review of vision-based safety systems for human-robot collaboration. *Procedia Cirp*, 72:111–116, 2018. 2
- [25] Jiangyong Huang, Silong Yong, Xiaojian Ma, Xiongkun Linghu, Puhao Li, Yan Wang, Qing Li, Song-Chun Zhu, Baoxiong Jia, and Siyuan Huang. An embodied generalist agent in 3d world. *arXiv preprint arXiv:2311.12871*, 2023. 2
- [26] Wenlong Huang, Chen Wang, Ruohan Zhang, Yunzhu Li, Jiajun Wu, and Li Fei-Fei. Voxposer: Composable 3d value maps for robotic manipulation with language models. In *CoRL*, 2023. 3
- [27] F elix Ingrand and Malik Ghallab. Deliberation for autonomous robots: A survey. *Artif. Intell.*, 247:10–44, 2017. 2
- [28] ISO 10218-1/2:2011. Robots and Robotic Devices Safety Requirements for Industrial Robots Part 1: Robots/Part 2: Robot Systems and Integration. Standard, International Organization for Standardization, 2011. 2, 4
- [29] ISO13482. Robots and robotic devices — safety requirements for personal care robots. *International Organization for Standardization*, 2014.
- [30] ISO/TS 15066:2016. Robots and Robotic Devices Collaborative Robots. Standard, International Organization for Standardization, 2016. 2, 4
- [31] Stephen James, Michael Bloesch, and Andrew J. Davison. Task-embedded control networks for few-shot imitation learning. In *CoRL*, 2018. 2
- [32] Yunfan Jiang, Agrim Gupta, Zichen Zhang, Guanzhi Wang, Yongqiang Dou, Yanjun Chen, Li Fei-Fei, Anima Anandkumar, Yuke Zhu, and Linxi Fan. VIMA: general robot manipulation with multimodal prompts. *arXiv preprint arXiv:2210.03094*, 2022. 2, 13
- [33] Mingyu Jin, Qinkai Yu, Dong Shu, Haiyan Zhao, Wenyue Hua, Yanda Meng, Yongfeng Zhang, and Mengnan Du. The impact of reasoning step length on large language models. In *ACL*, 2024. 2
- [34] Siddharth Karamcheti, Suraj Nair, Ashwin Balakrishna, Percy Liang, Thomas Kollar, and Dorsa Sadigh. Prismatic vlms: Investigating the design space of visually-conditioned language models. *arXiv preprint arXiv:2402.07865*, 2024. 2
- [35] Moo Jin Kim, Karl Pertsch, Siddharth Karamcheti, Ted Xiao, Ashwin Balakrishna, Suraj Nair, Rafael Rafailov, Ethan Foster, Grace Lam, Pannag Sanketi, Quan Vuong, Thomas Kollar, Benjamin Burchfiel, Russ Tedrake, Dorsa Sadigh, Sergey Levine, Percy Liang, and Chelsea Finn. Openvla: An open-source vision-language-action model. *arXiv preprint arXiv:2406.09246*, 2024. 1, 2, 3, 4, 5, 6, 13
- [36] Hema Swetha Koppula and Ashutosh Saxena. Learning spatio-temporal structure from RGB-D videos for human activity detection and anticipation. In *ICML*, 2013. 2
- [37] Hema Swetha Koppula and Ashutosh Saxena. Anticipating human activities using object affordances for reactive robotic response. *IEEE Trans. Pattern Anal. Mach. Intell.*, 38(1):14–29, 2016. 2
- [38] Oliver Kroemer, Scott Niekum, and George Konidaris. A review of robot learning for manipulation: Challenges, representations, and algorithms. *J. Mach. Learn. Res.*, 22:30:1–30:82, 2021. 2
- [39] Andrew J Kurdila and Pinhas Ben-Tzvi. *Dynamics and control of robotic systems*. John Wiley & Sons, 2019. 14
- [40] Przemyslaw A. Lasota, Terrence Fong, and Julie A. Shah. A survey of methods for safe human-robot interaction. *Found. Trends Robotics*, 5(4):261–349, 2017. 2
- [41] Przemyslaw A Lasota, Terrence Fong, Julie A Shah, et al. A survey of methods for safe human-robot interaction. *Foundations and Trends  in Robotics*, 5(4):261–349, 2017. 2
- [42] Sergey Levine, Peter Pastor, Alex Krizhevsky, Julian Ibarz, and Deirdre Quillen. Learning hand-eye coordination for robotic grasping with deep learning and large-scale data collection. *Int. J. Robotics Res.*, 37(4-5):421–436, 2018. 2
- [43] Xinghang Li, Minghuan Liu, Hanbo Zhang, Cunjun Yu, Jie Xu, Hongtao Wu, Chilam Cheang, Ya Jing, Weinan Zhang, Huaping Liu, et al. Vision-language foundation models as effective robot imitators. *arXiv preprint arXiv:2311.01378*, 2023. 2
- [44] Xiang Li, Cristina Mata, Jongwoo Park, Kumara Kahatapitiya, Yoo Sung Jang, Jinghuan Shang, Kanchana Ranasinghe, Ryan Burgert, Mu Cai, Yong Jae Lee, and Michael S. Ryoo. Llara: Supercharging robot learning data for vision-language policy. *arXiv preprint arXiv:2406.20095*, 2024. 3, 6, 13
- [45] Aishan Liu, Xianglong Liu, Jiabin Fan, Yuqing Ma, Anlan Zhang, Huiyuan Xie, and Dacheng Tao. Perceptual-sensitive GAN for generating adversarial patches. In *AAAI*, 2019. 3, 13
- [46] Bo Liu, Yifeng Zhu, Chongkai Gao, Yihao Feng, Qiang Liu, Yuke Zhu, and Peter Stone. LIBERO: benchmarking knowledge transfer for lifelong robot learning. In *NeurIPS*, 2023. 6, 7, 8, 13, 14, 16
- [47] Haotian Liu, Chunyuan Li, Yuheng Li, and Yong Jae Lee. Improved baselines with visual instruction tuning. In *CVPR*, 2024. 2
- [48] Haotian Liu, Chunyuan Li, Qingyang Wu, and Yong Jae Lee. Visual instruction tuning. In *NeurIPS*, 2024. 2
- [49] Ilya Loshchilov and Frank Hutter. Decoupled weight decay regularization. In *ICLR*, 2019. 6
- [50] Alessandro De Luca, Alin Albu-Sch affer, Sami Haddadin, and Gerd Hirzinger. Collision detection and safe reaction with the DLR-III lightweight manipulator arm. In *IROS*, 2006. 2
- [51] Aleksander Madry, Aleksandar Makelov, Ludwig Schmidt, Dimitris Tsipras, and Adrian Vladu. Towards deep learning models resistant to adversarial attacks. In *ICLR*, 2018. 3, 5

- [52] Jim Mainprice and Dmitry Berenson. Human-robot collaborative manipulation planning using early prediction of human motion. In *IROS*, 2013. 2
- [53] Matthew T. Mason. *Mechanics of Robotic Manipulation*. MIT Press, 2001. 2
- [54] Matthew T. Mason. Toward robotic manipulation. *Annu. Rev. Control. Robotics Autom. Syst.*, 1:1–28, 2018. 2
- [55] Oier Mees, Lukás Hermann, and Wolfram Burgard. What matters in language conditioned robotic imitation learning over unstructured data. *IEEE Robotics Autom. Lett.*, 7(4): 11205–11212, 2022. 2
- [56] Vivek G Moudgal, Kevin M Passino, and Stephen Yurkovich. Rule-based control for a flexible-link robot. *IEEE Trans. on Control Sys. Tech.*, 2(4):392–405, 1994. 2
- [57] Richard M. Murray, Zexiang Li, and S. Shankar Sastry. *A mathematical introduction to robotics manipulation*. CRC Press, 1994. 2
- [58] Adam Paszke, Sam Gross, Francisco Massa, Adam Lerer, James Bradbury, Gregory Chanan, Trevor Killeen, Zeming Lin, Natalia Gimelshein, Luca Antiga, Alban Desmaison, Andreas Kopf, Edward Yang, Zachary DeVito, Martin Raison, Alykhan Tejani, Sasank Chilamkurthy, Benoit Steiner, Lu Fang, Junjie Bai, and Soumith Chintala. Pytorch: An imperative style, high-performance deep learning library. In *NeurIPS*, 2019. 7
- [59] Lerrel Pinto and Abhinav Gupta. Supersizing self-supervision: Learning to grasp from 50k tries and 700 robot hours. In *ICRA*, 2016. 2
- [60] Vitchyr Pong, Murtaza Dalal, Steven Lin, Ashvin Nair, Shikhar Bahl, and Sergey Levine. Skew-fit: State-covering self-supervised reinforcement learning. In *ICML*, 2020. 2
- [61] Xiangyu Qi, Kaixuan Huang, Ashwinee Panda, Peter Henderson, Mengdi Wang, and Prateek Mittal. Visual adversarial examples jailbreak aligned large language models. In *AAAI*, 2024. 3
- [62] Mahmood Sharif, Sruti Bhagavatula, Lujo Bauer, and Michael K. Reiter. Accessorize to a crime: Real and stealthy attacks on state-of-the-art face recognition. In *ACM SIGSAC*, 2016. 3
- [63] Michael H. Smith and L. Stephen Coles. Design of a low cost, general purpose robot. In *IJCAI*, 1973. 2
- [64] Jiawei Su, Danilo Vasconcellos Vargas, and Kouichi Sakurai. One pixel attack for fooling deep neural networks. *IEEE Trans. Evol. Comput.*, 23(5):828–841, 2019. 3
- [65] Christian Szegedy, Wojciech Zaremba, Ilya Sutskever, Joan Bruna, Dumitru Erhan, Ian J. Goodfellow, and Rob Fergus. Intriguing properties of neural networks. In *ICLR*, 2014. 3
- [66] Chen Tang, Ben Abbatematteo, Jiaheng Hu, Rohan Chandra, Roberto Martín-Martín, and Peter Stone. Deep reinforcement learning for robotics: A survey of real-world successes. *arXiv preprint arXiv:2408.03539*, 2024. 2
- [67] Octo Model Team, Dibya Ghosh, Homer Walke, Karl Pertsch, Kevin Black, Oier Mees, Sudeep Dasari, Joey Hejna, Tobias Kreiman, Charles Xu, Jianlan Luo, You Liang Tan, Lawrence Yunliang Chen, Pannag Sanketi, Quan Vuong, Ted Xiao, Dorsa Sadigh, Chelsea Finn, and Sergey Levine. Octo: An open-source generalist robot policy. *arXiv preprint arXiv:2405.12213*, 2024. 2, 3
- [68] Florian Tramèr. Detecting adversarial examples is (nearly) as hard as classifying them. In *ICML*, 2022. 3
- [69] Florian Tramèr, Nicholas Carlini, Wieland Brendel, and Aleksander Madry. On adaptive attacks to adversarial example defenses. In *NeurIPS*, 2020. 6
- [70] Valeria Villani, Fabio Pini, Francesco Leali, and Cristian Secchi. Survey on human–robot collaboration in industrial settings: Safety, intuitive interfaces and applications. *Mechatronics*, 55:248–266, 2018. 2
- [71] Christian Vogel, Christoph Walter, and Norbert Elkmann. A projection-based sensor system for safe physical human-robot collaboration. In *IROS*, 2013. 2, 7
- [72] Homer Rich Walke, Kevin Black, Tony Z. Zhao, Quan Vuong, Chongyi Zheng, Philippe Hansen-Estruch, Andre Wang He, Vivek Myers, Moo Jin Kim, Max Du, Abraham Lee, Kuan Fang, Chelsea Finn, and Sergey Levine. Bridgedata V2: A dataset for robot learning at scale. In *CoRL*, 2023. 6, 8, 13
- [73] Taowen Wang, Yiyang Liu, James Chenhao Liang, Yiming Cui, Yuning Mao, Shaoliang Nie, Jiahao Liu, Fuli Feng, Zenglin Xu, Cheng Han, et al. M²pt: Multimodal prompt tuning for zero-shot instruction learning. In *EMNLP*, 2024. 1, 2
- [74] Zhibo Wang, Siyan Zheng, Mengkai Song, Qian Wang, Alireza Rahimpour, and Hairong Qi. advpattern: Physical-world attacks on deep person re-identification via adversarially transformable patterns. In *ICCV*, 2019. 3
- [75] Zixiang Wang, Hao Yan, Zhuoyue Wang, Zhengjia Xu, Zhizhong Wu, and Yining Wang. Research on autonomous robots navigation based on reinforcement learning. In *RAIIC*, 2024. 2
- [76] Zhijie Wang, Zhehua Zhou, Jiayang Song, Yuheng Huang, Zhan Shu, and Lei Ma. Towards testing and evaluating vision-language-action models for robotic manipulation: An empirical study. *arXiv preprint arXiv:2409.12894*, 2024. 1
- [77] Junjie Wen, Yichen Zhu, Jinming Li, Minjie Zhu, Kun Wu, Zhiyuan Xu, Ran Cheng, Chaomin Shen, Yaxin Peng, Feifei Feng, et al. Tinyvla: Towards fast, data-efficient vision-language-action models for robotic manipulation. *arXiv preprint arXiv:2409.12514*, 2024. 1
- [78] Wikipedia contributors. Finch (film) — Wikipedia, the free encyclopedia. [https://en.wikipedia.org/w/index.php?title=Finch_\(film\)&oldid=1249481595](https://en.wikipedia.org/w/index.php?title=Finch_(film)&oldid=1249481595), 2024. [Online; accessed 5-November-2024]. 1
- [79] Chen Henry Wu, Jing Yu Koh, Ruslan Salakhutdinov, Daniel Fried, and Aditi Raghunathan. Adversarial attacks on multimodal agents. *arXiv preprint arXiv:2406.12814*, 2024. 3
- [80] Kaidi Xu, Gaoyuan Zhang, Sijia Liu, Quanfu Fan, Mengshu Sun, Hongge Chen, Pin-Yu Chen, Yanzhi Wang, and Xue Lin. Adversarial t-shirt! evading person detectors in a physical world. In *ECCV*, 2020. 3
- [81] Weilin Xu, David Evans, and Yanjun Qi. Feature squeezing: Detecting adversarial examples in deep neural networks. In *NDSS*, 2018. 8, 15
- [82] Zhiyang Xu, Chao Feng, Rulin Shao, Trevor Ashby, Ying Shen, Di Jin, Yu Cheng, Qifan Wang, and Lifu Huang. Visionflan: Scaling human-labeled tasks in visual instruction tuning. *arXiv preprint arXiv:2402.11690*, 2024. 1

- [83] Yuchen Zhang and Percy Liang. Defending against whitebox adversarial attacks via randomized discretization. In *AISTATS*, 2019. 8, 15
- [84] Yaoyuan Zhang, Yu-an Tan, Tian Chen, Xinrui Liu, Quanxin Zhang, and Yuanzhang Li. Enhancing the transferability of adversarial examples with random patch. In *IJCAI*, 2022. 8, 13
- [85] Bo Zhao, Boya Wu, Muyang He, and Tiejun Huang. Svit: Scaling up visual instruction tuning. *arXiv preprint arXiv:2307.04087*, 2023. 2
- [86] Yuanyang Zhu, Zhi Wang, Chunlin Chen, and Daoyi Dong. Rule-based reinforcement learning for efficient robot navigation with space reduction. *IEEE/ASME Trans. on Mechatronics*, 27:846–857, 2021. 2
- [87] Brianna Zitkovich, Tianhe Yu, Sichun Xu, Peng Xu, Ted Xiao, Fei Xia, Jialin Wu, Paul Wohlhart, Stefan Welker, Ayzaan Wahid, Quan Vuong, Vincent Vanhoucke, Huong T. Tran, Radu Soricut, Anikait Singh, Jaspiar Singh, Pierre Sermanet, Pannag R. Sanketi, Grecia Salazar, Michael S. Ryoo, Krista Reymann, Kanishka Rao, Karl Pertsch, Igor Mordatch, Henryk Michalewski, Yao Lu, Sergey Levine, Lisa Lee, Tsang-Wei Edward Lee, Isabel Leal, Yuheng Kuang, Dmitry Kalashnikov, Ryan Julian, Nikhil J. Joshi, Alex Irpan, Brian Ichter, Jasmine Hsu, Alexander Herzog, Karol Hausman, Keerthana Gopalakrishnan, Chuyuan Fu, Pete Florence, Chelsea Finn, Kumar Avinava Dubey, Danny Driess, Tianli Ding, Krzysztof Marcin Choromanski, Xi Chen, Yevgen Chebotar, Justice Carbajal, Noah Brown, Anthony Brohan, Montserrat Gonzalez Arenas, and Kehang Han. RT-2: vision-language-action models transfer web knowledge to robotic control. In *CoRL*, 2023. 2, 3

SUMMARY OF THE APPENDIX

This appendix contains additional experimental results and discussions of our work, organized as:

- §S1 includes additional simulation results for **black-box attacks** with different VLA-based models.
- §S2 provides **targeted attack supply results**, investigating TMA across various action magnitudes and patch sizes.
- §S3 explains tasks adopted for **real-world experiments**.
- §S4 studies failure cases, providing an in-depth analysis of the limitations of the proposed methods.
- §S5 outlines the **evaluation details** conducted in the LIBERO [46] simulation environment.
- §S6 supplies additional information on **diagnostic experiments**.
- §S7 outlines the parameter configurations used in **robustness evaluations**.
- §S8 visualizes **more qualitative results**.
- §S9 provides discussions on **future directions**, highlighting potential areas for further research.

S1. Black-box Attack Results

This section examines the black-box settings of our proposed attacks, focusing on evaluating the transferability of the proposed patch attack. To this end, we include another VLA-based model in our experiment: **LLaRA** [44].

Setup. For the LLaRA black-box experiment, we generate adversarial patch from simulation (*i.e.* openvla-7B-libero-long [35] model with LIBERO Long [46] dataset) and physical (*i.e.* openvla-7B [35] model with BridgeData V2 [72] dataset). These patches are then pasted at the top-left corner of the image in the VIMA [32] scenario.

Table S1. **LLaRA [44] black-box results.** We report failure rates (%) in VIMA [32] scenario. Simulation and physical represent the same experiment setup as provided in §4.1. The FR (\uparrow) is highlighted in **best** and **second best** for each difficulty.

Setup	Objective	DoF	Task Difficulty			
			L1	L2	L3	L4
LLaRA (D-inBC + Aux (D) + Oracle)			10.0	11.9	20.8	66.2
Simulation	Untargeted	DoF ₁	15.8	20.8	29.2	67.5
	Untargeted	DoF ₁₋₃	15.8	16.5	27.5	70.0
	UADA	DoF ₁	15.0	18.8	27.1	71.3
	UPA	DoF ₁₋₃	<u>15.9</u>	19.1	<u>28.8</u>	71.1
Physical	Untargeted	DoF ₁	13.8	23.5	26.2	76.4
	Untargeted	DoF ₁₋₃	14.2	<u>26.4</u>	27.6	74.7
	UADA	DoF ₁	16.3	27.2	28.5	<u>76.1</u>
	UPA	DoF ₁₋₃	12.7	25.6	28.7	72.1

Results. Across the four task difficulty tasks (L1-L4) in VIMA [32], adversarial patches significantly increase the failure rate (See Tab. S1) compared to the benign result of LLaRA (D-inBC + Aux (D) + Oracle). For L1, the UPA

objective under the simulation setting increases the failure rate by 6.3% (16.3% *v.s.* 10.0%). For L2, the adversarial patch generated with Untargeted objective under physical setup achieves the highest failure rate, increasing the failure rate by 15.3% (27.2% *v.s.* 11.9%). For L3, Untargeted Action Discrepancy Attack (UADA) under the physical setting demonstrates strong effectiveness, increasing the failure rate by 8.4% (29.2% *v.s.* 20.8%). Finally, for L4, the physical setting with the Untargeted objective effectively increases the failure rate by 10.2% (76.4% *v.s.* 66.2%).

S2. Targeted Attack supply Results

In this section, we explore Targeted Manipulation Attack (TMA) with different action magnitude targets and investigate the impact of patch size on failure rate.

S2.1. Investigation of Action Magnitude

To further explore the action manipulation capabilities of TMA, we conduct experiments targeting varying magnitudes to assess its effectiveness across different scenarios.

Setup. We conduct experiments attack at DoF₁ and utilize various action magnitudes (*i.e.* 0.5, -0.5, 1.0, -1.0) as the attack targets under simulation and physical settings.

Table S2. **Different Magnitude results.** Average failure rate (%) is reported in 4 LIBERO simulation tasks. The initial AFR across the four tasks is 23.5%.

Target Action	Metric	Action Magnitude			
		0.5	-0.5	1.0	-1.0
Simulation	L1	0.072	0.049	0.132	0.107
	AFR	82.5	87.8	78.4	74.2
Physical	L1	0.055	0.071	0.103	0.121
	AFR	62.5	68.8	63.8	58.3

Results. The results are presented in Tab. S2. In the simulation setup, the highest AFR (87.8%) is achieved at a target magnitude of -0.5, representing a substantial increase of 64.3% compared to the initial AFR (87.8% *v.s.* 23.5%). Similarly, in the physical setup, the target magnitude of -0.5 yields the highest AFR of 68.8%. These findings highlight the superior manipulation capability and disruptive effectiveness of TMA.

S2.2. Investigation of Patch Size

Acknowledging the trade-off between stealth and attack effectiveness [8, 45, 84], in this section, we further examine the impact of different patch sizes on AFR to explore how this balance influences performance.

Table S3 presents the average failure rates of the TMA attack on DoF₁ with a target action magnitude of 0 under the physical setup. The results indicate that the failure rate increases as the patch size grows. Balancing stealth and attack efficiency, we adopt a patch size of 5% as the primary attack configuration for all experiments.

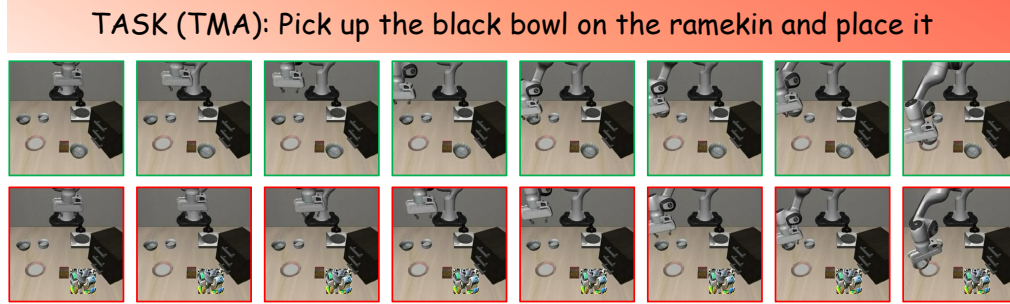


Figure S1. **Redundant DoF in a Failure Case.** The first row is the **benign** scenario, while the second row illustrates the **adversarial** scenario. In the adversarial scenario, the adversarial patch is generated by targeting DoF₄ within the simulation setup. In this task, orientation (*i.e.* DoF₄₋₆) is identified as a redundant DoF since the task completion does not require any changes in orientation. As a result, the DoF₄ attack, which focuses on orientation, fails to disrupt the task’s execution.

Table S3. **Patch Size.** We compare the average failure rates across four LIBERO [46] tasks using different patch sizes. Patch size (%) indicates the proportion of the adversarial patch to the input image.

Setup	Patch Size (%)	AFR (%)
Physical	3	72.4
	5	89.1
	7	92.4
	10	93.6

S3. Details of Real-world Experiments

We design four tasks to evaluate the impact of adversarial samples on task failure rates in real-world scenarios. The specific tasks include “put the carrot on the plate”, “put the corn on the plate”, “put the carrot into the bowl”, and “flip the pot upright”. To fairly evaluate the performance of our attack, we only consider tasks where the VLA model operates successfully, excluding failure cases. We then introduce the adversarial patch to assess its impact. This leads to an average task failure rate of 43%, underscoring the significant disruptive potential of adversarial samples on robotic tasks.

S4. Failure Case Analysis

This section analyzes the attack failure cases to gain deeper insights into robot manipulation and highlight the critical role of DoF targets on task failure.

We analyze most of attack failure cases and find that certain DoFs are redundant in task execution. In Fig. S1, the adversarial patch targeting DoF₄ with a value of 0 fails to disrupt the execution of the task. This failure can be attributed to the fact that DoF₄ controls the orientation along the x-axis, which is redundant for grasping objects such as bowls in the context of this task. As a result, attacks targeting **redundant DoF of the task** [39] are less likely to disrupt successful execution effectively. This observation underscores the importance of task-specific considerations when designing adversarial attacks on robotic systems.

Table S4. **Parameter Diagnostic Results.** Four distinct α and β combination results. We report the average failure rate of four tasks in LIBERO [46].

Setup	α	β	AFR (%)
Simulation	0.2	0.8	86.5
	0.4	0.6	90.5
	0.6	0.4	89.4
	0.8	0.2	93.4

S5. More Evaluation Details

This section supplies details on the evaluation of the three attacks in §4.1. To rigorously assess the effectiveness of attacks and minimize task failures arising from random placement of adversarial patches that obscure critical task-relevant objects, we identify base left-corner locations for patch placement specific to each of the four tasks in LIBERO [46]. These locations are further extended by shifting the x and y coordinates by ± 3 pixels, resulting in a total of 9 placement locations. For the Spatial task, the base point is set as (120, 160). For the Object task, the base point is (30, 150). Similarly, the base point is (15, 158) for the Goal task and (5, 160) for the Long task. This approach ensures an accurate evaluation of adversarial patches on task performance.

S6. More Diagnostic Experiment Details

We perform diagnostic experiments to assess the influence of the hyperparameters α and β in UPA. As shown in Tab. S4, when $\alpha = 0.8$ and $\beta = 0.2$, UPA achieves the highest average score of 93.4 across the four LIBERO [46] tasks among all tested configurations. This result indicates that this specific combination optimally balances the trade-offs between direction and magnitude adjustments governed by α and β , establishing it as the most effective choice.

S7. More Robustness Evaluation Details

In this section, we provide a detailed parameter setting of conducted robustness evaluation in §4.4. Specifically, we assess the effectiveness of four commonly employed defense

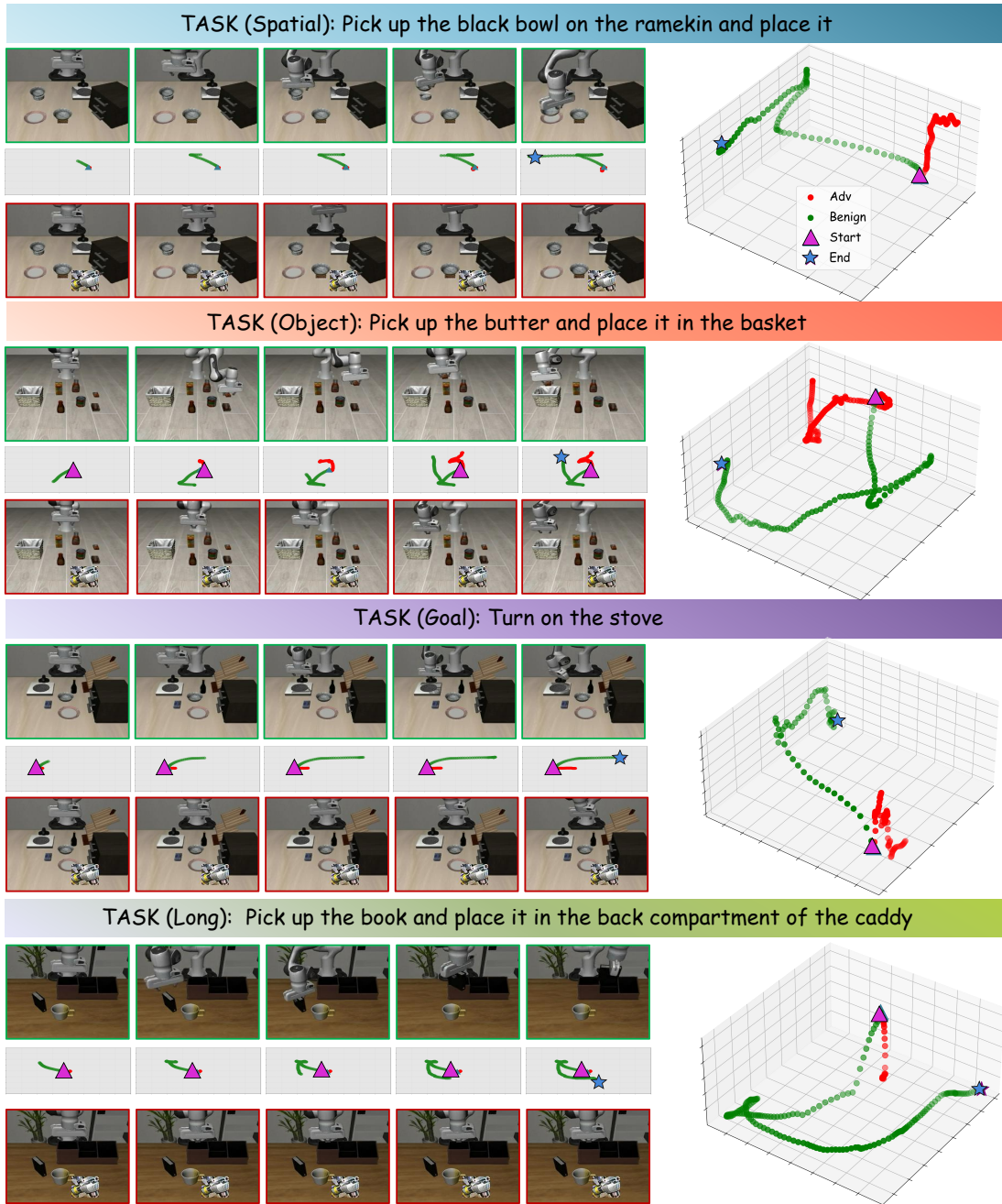


Figure S2. **UADA Qualitative Results** The figure illustrates the 3D and 2D trajectories for both benign ● and adversarial ● scenarios, highlighting the impact of the adversarial patch at each time step. We visualize the start point, marked as ▲, and the endpoint, marked as ★.

techniques, including JPEG compression [18], bit-depth reduction [81], median blur [81], and Gaussian noise [83]. **JPEG compression** applies compression algorithms to the input images prior to feeding them into the depth estimation network, aiming to disrupt adversarial patterns. We test compression quality levels ranging from 50 to 10, with lower quality levels corresponding to higher compression rates. **Gaussian noise** introduces zero-mean Gaussian noise to the input image, leveraging its randomness to counteract the

structured nature of adversarial perturbations. The standard deviation of the noise varies from 0.01 to 0.1, with higher values introducing stronger noise. **Median blur** smooths the image by replacing each pixel value with the median of its surrounding pixels, using square kernel sizes from 3 to 9; larger kernel sizes produce stronger smoothing effects. **Bit-depth reduction** remaps the standard 8-bit depth of RGB channels to smaller bit depths, reducing the color space and potentially disrupting adversarial perturbations. We evaluate

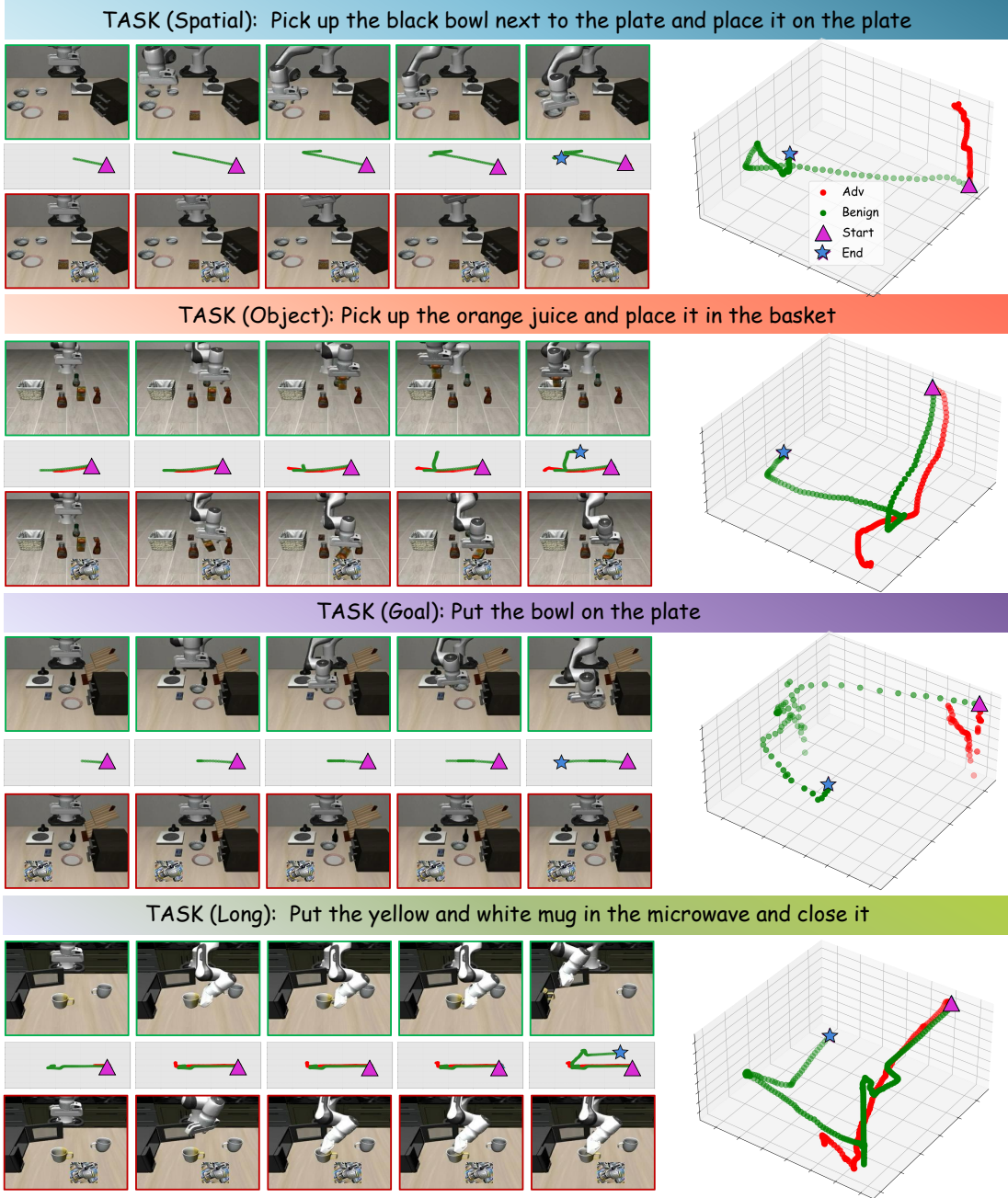


Figure S3. **UPA Qualitative Results** The figure illustrates the 3D and 2D trajectories for both benign ● and adversarial ● scenarios, highlighting the impact of the adversarial patch at each time step. We visualize the start point, marked as ▲, and the endpoint, marked as ★

cases with bit depths ranging from 6 bits to 3 bits. These defense techniques are evaluated to understand the robustness of our attack (results see in Fig. 4).

S8. More Qualitative Results

This section presents additional qualitative results for each of the three attack objectives, complementing results in §4.2 and offering deeper insights into the effectiveness of our adversarial attacks. Specifically, the results of UADA, UPA,

and TMA are shown in Fig. S2, S3, and S4, respectively. These qualitative results reveal significant deviations in the adversarial trajectories of the proposed methods across all four LIBERO tasks compared to the benign trajectories. Specifically, UADA induces substantial action discrepancies while diverging sharply from the benign trajectory, highlighting its disruptive impact. For UPA, a significant position deviation is observed on the spatial task [46], where the adversarial trajectory deviates significantly from the benign

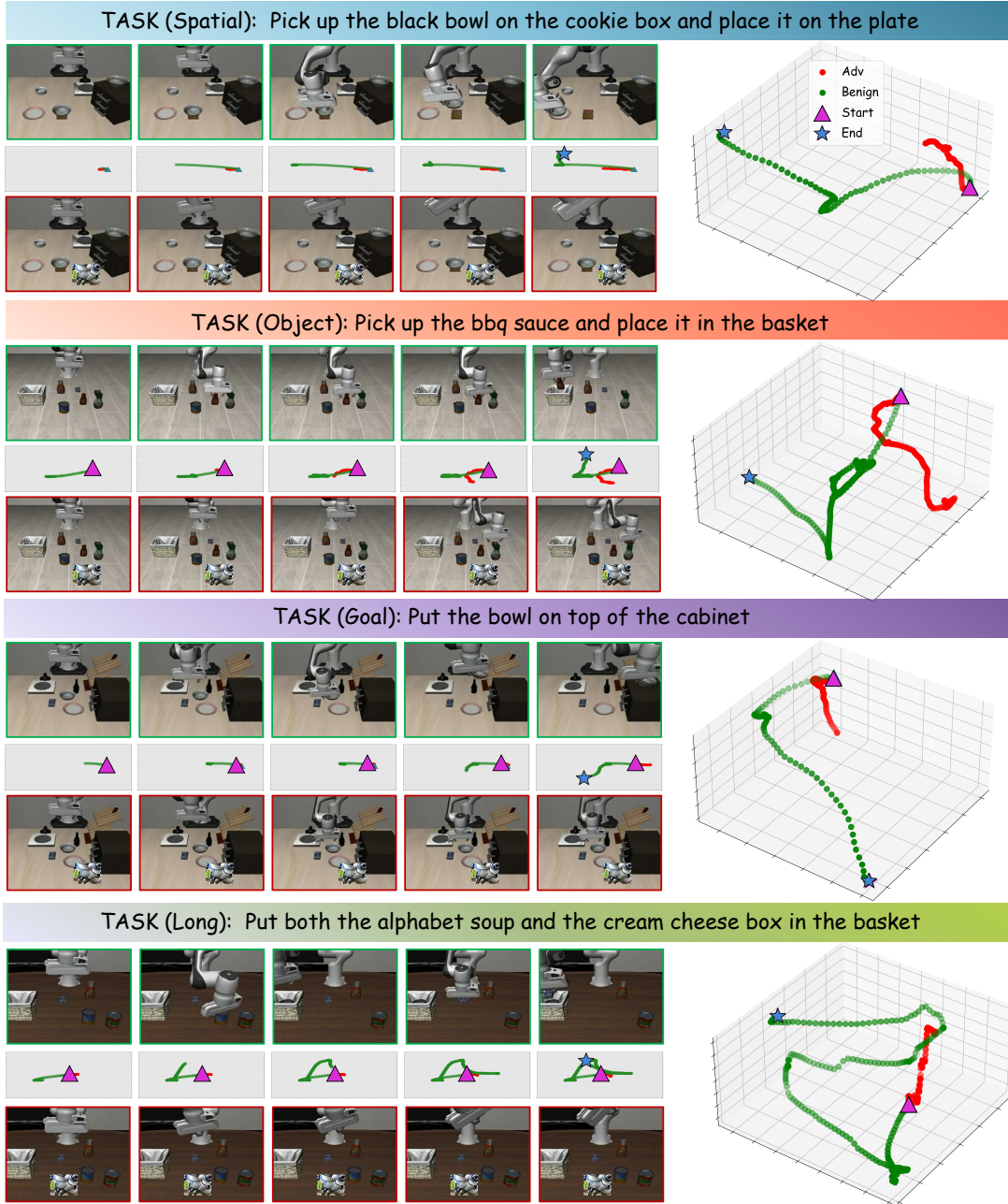


Figure S4. **TMA Qualitative Results** The figure illustrates the 3D and 2D trajectories for both benign ● and adversarial ● scenarios, highlighting the impact of the adversarial patch at each time step. We visualize the start point, marked as ▲, and the endpoint, marked as ★

trajectory, ultimately causing task failure. In contrast, the TMA exhibits a smaller action amplitude, successfully manipulating the robot's behavior and resulting in task failure. These findings highlight the distinct impacts and underlying mechanisms of the three attack methods.

S9. Future direction

Future research on attacks against VLA-based models can potentially be conducted on two key objectives: enhancing camouflage and ensuring practical feasibility. Improving

camouflage involves reducing detection probability by generating adversarial patches that seamlessly integrate with the environment, leveraging natural patterns and context-aware design. Furthermore, future efforts should avoid targeting redundant DoF and instead concentrate on critical components that are most likely to disrupt task performance. This can be achieved by leveraging task-specific knowledge and employing advanced optimization techniques to maximize the effectiveness of such attacks while aligning with real-world physical constraints.